Shape Evolution of Layer-Structured Bismuth Oxychloride Nanostructures via Low-Temperature Chemical Vapor Transport

Hailin Peng,[†] Candace K. Chan,[‡] Stefan Meister,[†] Xiao Feng Zhang,[§] and Yi Cui*,[†]

Department of Materials Science and Engineering and Department of Chemistry, Stanford University, Stanford, California 94305, and Electron Microscope Division, Hitachi High Technologies America, Inc., 5100 Franklin Drive, Pleasanton, California 94588

Received July 27, 2008. Revised Manuscript Received November 10, 2008

Bismuth oxychloride (BiOCl) is a wide bandgap semiconductor used in cosmetics, pharmaceuticals, battery cathode, photocatalysis, and photoelectrochemical devices. We report here a facile low-temperature vapor-phase synthesis route for the direct grown of single crystalline BiOCl nanostructures on various substrates. We achieved control of a variety of morphologies including nanobelts, nanowires, nanoflowers, nanoflakes, and platelets.

Introduction

Bismuth oxychloride (BiOCl) is a wide bandgap semiconductor (E_g = 3.46 eV) with a tetragonal PbFCl-type structure (space group *P*4/*nmm*; No. 129). BiOCl crystallizes into unique layered structures consisting of [Cl−Bi−O−Bi−Cl] sheets stacked together by the nonbonding interaction through the Cl atoms along the *c*-axis. In each [Cl−Bi−O−Bi−Cl] layer, a bismuth center is surrounded by four oxygen and four chlorine atoms in an asymmetric decahedral geometry. The strong intralayer bonding and the weak interlayer van der Waals interaction gives rise to highly anisotropic structural, electrical, optical, and mechanical properties, which have made BiOCl attractive in applications such as cosmetics, pharmaceuticals,[1,2] battery cathodes, photocatalysis,[3] and photoelectrochemical devices.[4] For example, BiOCl has been used in cosmetics, pigment plastics, and paints as a pearl luster pigment with extremely low toxicity for at least 50 years because it provides excellent whiteness and brightness as well as having a smooth texture. The tetragonal bipyramidal crystal geometry of BiOCl can be usually flattened into flakes or platelets with a high aspect ratio. Light between the semitransparent BiOCl flakes is reflected and multiplied, creating an impressive deep luster characteristic of natural pearls. The bonding anisotropy also suggests that there are no surface dangling bonds except at the edge of the layers and that photoexcited antibonding states do not weaken the O−Bi−Cl bond, enabling good photostability. Owing to the unique layered structure and high photocorrosion stabilities in the presence of redox pairs, BiOCl has recently been shown as a novel material for photocatalysis and photoelectrochemical (PEC) cells.[3−5] In addition, BiOCl catalysts show high activity and high selectivity to the oxidative cracking of *n*-butane and oxidative coupling of methane (OCM) reactions.[6] BiOCl can be perfectly cleaved along the [001] plane, giving a surface layer of chlorine atoms, which is a key element in the C−H activation of alkanes.[7]

One-dimensional nanowire (NW) and nanobelt (NB) structures can enhance the activity in chemical catalysis and photocatalysis because of their large surface-to-volume ratios.[8] NWs and NBs structures can also afford better materials for photoelectrochemical cells because NWs and NBs have a large surface area for charge carrier separation and fast ion intercalation while maintaining efficient charge carrier transport.[9−11] In addition, nanostructures can provide a good system for studying the shape- and size-dependent properties with respect to the pigment field. BiOCl pigments with an aspect ratio of 10−15 show low luster and very good skin feeling and are used as fillers in cosmetics. Crystals with higher aspect ratio show strong luster and are mainly used for nail polish. The color of BiOCl nanoparticles can vary from pale yellow to dark orange depending on the size of the particles.[12]

Most of the reported methods for the synthesis of BiOCl nanostructures are wet chemical methods.[3,5,12−19] Recently BiOCl lamellae were synthesized via a sonochemical method

* To whom correspondence should be addressed. Email: yicui@stanford.edu.
[†] Department of Materials Science and Engineering, Stanford University.
[‡] Department of Chemistry, Stanford University.
[§] Hitachi High Technologies America, Inc.

(1) Rotmensch, J.; Whitlock, J. L.; Dietz, M. L.; Hines, J. J.; Reba, R. C.; Horwitz, E. P.; Harper, P. V. *Abstr. Pap. Am. Chem. Soc.* **1998**, *216*, U926.
(2) Briand, G. G.; Burford, N. *Chem. Rev.* **1999**, *99*, 2601.
(3) Zhang, K. L.; Liu, C. M.; Huang, F. Q.; Zheng, C.; Wang, W. D. *Appl. Catal., B* **2006**, *68*, 125.
(4) Poznyak, S. K. *Electrochim. Acta* **1990**, *35*, 1941.
(5) Zhang, X.; Ai, Z. H.; Jia, F. L.; Zhang, L. Z. *J. Phys. Chem. C* **2008**, *112*, 747.
(6) Kijima, N.; Matano, K.; Saito, M.; Oikawa, T.; Konishi, T.; Yasuda, H.; Sato, T.; Yoshimura, Y. *Appl. Catal., A* **2001**, *206*, 237.
(7) Ueda, W.; Isozaki, T.; Sakyu, F.; Nishiyama, S.; Morikawa, Y. *Bull. Chem. Soc. Jpn.* **1996**, *69*, 485.
(8) Wu, Y. Y.; Yan, H. Q.; Yang, P. D. *Topics Catal.* **2002**, *19*, 197.
(9) Tian, B.; Zheng, X.; Kempa, T. J.; Fang, Y.; Yu, N.; Yu, G.; Huang, J.; Lieber, C. M. *Nature* **2007**, *449*, 885.
(10) Law, M.; Greene, L. E.; Johnson, J. C.; Saykally, R.; Yang, P. D. *Nat. Mater.* **2005**, *4*, 455.
(11) Chan, C. K.; Peng, H. L.; Liu, G.; McIlwrath, K.; Zhang, X. F.; Huggins, R. A.; Cui, Y. *Nat. Nanotechnol.* **2008**, *3*, 31.
(12) Henle, J.; Simon, P.; Frenzel, A.; Scholz, S.; Kaskel, S. *Chem. Mater.* **2007**, *19*, 366.
(13) Li, L. S.; Sun, N. J.; Huang, Y. Y.; Qin, Y.; Zhao, N.; Gao, J. N.; Li, M. X.; Zhou, H. H.; Qi, L. M. *Adv. Funct. Mater.* **2008**, *18*, 1194.

10.1021/cm802041g CCC: $40.75
Published on Web 12/19/2008

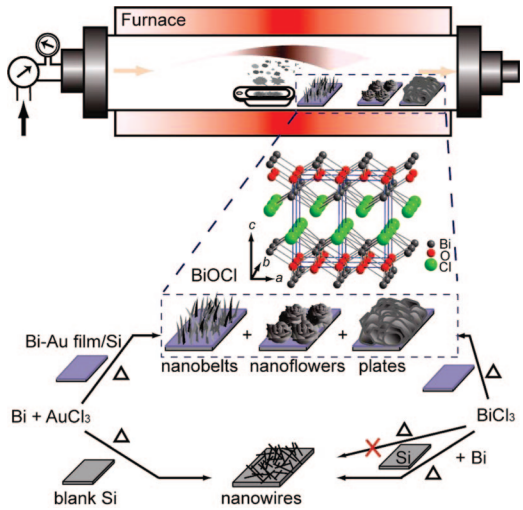

Figure 1. Chemical vapor transport approach as utilized for the controlled growth of BiOCl nanostructures.

in a surfactant/ligand-free solution.[18] A solvothermal method was used previously for producing BiOCl NBs.[20] Bismuth oxyhalide nanoparticles have also been prepared in reverse microemulsions.[12] Vapor-phase synthesis has been shown to be a powerful method for the synthesis of a variety of NW structures and heterostructures, although this method has not yet been applied to BiOCl nanostructures.[21−23] Herein, we exploit a direct vapor phase synthesis of high quality BiOCl nanostructures by vapor transport of a $AuCl_3$/Bi mixture or $BiCl_3$ powders at relatively low temperature (250 °C). BiOCl nanostructures could be directly grown on various substrates as a densely packed film. BiOCl nanostructures exhibit a variety of morphologies including NWs, NBs, nanoflowers, nanoflakes, and platelets. The strategy utilized for controllable growth of BiOCl morphologies is illustrated in Figure 1. We achieved the control of these morphologies by substrate temperature, evaporation source, and catalyst.

Experimental Section

(1) Growth Substrate Preparation. Three different growth substrates were prepared, using the following methods: (a) For bare silicon ⟨100⟩ substrate, silicon ⟨100⟩ wafer chips were etched in a 2% HF solution for 5 min to remove the intrinsic silicon oxide layer, followed by thorough rinsing with deionized water and drying in a stream of nitrogen gas. (b) For Bi/Au-covered Si ⟨100⟩ substrate, a clean Si ⟨100⟩ wafer with intrinsic oxide was coated with 20 nm Bi first and then 5 nm Au by electron beam evaporation. (c) For Bi/Au-covered glass slide, precleaned glass slides were coated with 5 nm Bi first and then 5 nm Au by electron beam evaporation. All the substrates were stored under inert atmosphere in a glovebox.

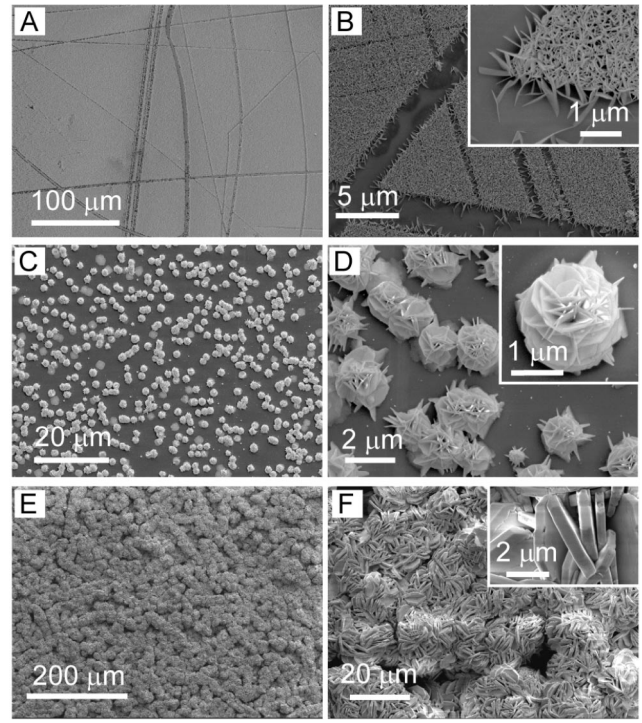

Figure 2. Typical SEM images of as-grown BiOCl nanostructures with different morphologies at different growth temperature zones: (A, B) nanobelts at 250 °C; (C, D) roselike nanoflowers at ∼200 °C; (E, F) platelets at 150 °C.

(2) Nanostructure Growth. The BiOCl nanostructures were synthesized in a 12-in. horizontal tube furnace (Lindberg/Blue M) equipped with a 1 in. diameter quartz tube (Figure 1). The source materials, $AuCl_3$ (99%, Sigma-Aldrich) and Bi (99.99+%, Sigma-Aldrich) powder mixture, were placed in an alumina boat in the center of the furnace. N_2 (99.999%) acted as a carrier gas. The BiOCl nanostructures were grown on the targeted substrates placed downstream at the different locations with different temperatures. Typical synthesis conditions are as follows: 0.06 g of $AuCl_3$, 0.05 g of Bi, furnace temperature setpoint at 250 °C, growth time = 1 h, gas flow = 120 sccm, and growth pressure = 1 atm. $BiCl_3$ (98+%, Alfa Aesar) powder is an alternatively efficient source. Before loading in the tube furnace, the surface of the $BiCl_3$ powder was moisturized and hydrolyzed with several drops (0.4−0.8 mL) of deionized water.

(3) Structural Characterization. The nanostructures were characterized in an FEI Sirion scanning electron microscope (SEM) and a Hitachi 300 kV H-9500 and Philips 200 KV CM20 transmission electron microscope (TEM). Chemical analysis was done using energy dispersive X-ray spectrometry (EDS) in both SEM and TEM. Tapping-mode atomic force microscopy (AFM) images were recorded on Nanoscope IIIA (Digital Instruments) in air under ambient conditions. X-ray diffraction (XRD) measurements were carried out with a PANalytical X'Pert PRO X-ray diffraction system.

Results and Discussion

(1) Shape Evolution of the BiOCl Nanostructures. The substrate temperature plays an important role in the formation of BiOCl nanostructures with different morphologies. Figure 2 shows typical SEM images of as-grown products with different morphologies on the substrates placed at different

(14) Deng, Z. T.; Tang, F. Q.; Muscat, A. J. *Nanotechnology* **2008**, *19*, 295705.
(15) Henle, J.; Kaskel, S. *J. Mater. Chem.* **2007**, *17*, 4964.
(16) Chen, X. Y.; Huh, H. S.; Lee, S. W. *J. Solid State Chem.* **2007**, *180*, 2510.
(17) Geng, J.; Hou, W. H.; Lv, Y. N.; Zhu, J. J.; Chen, H. Y. *Inorg. Chem.* **2005**, *44*, 8503.
(18) Zhu, L. Y.; Xie, Y.; Zheng, X. W.; Yin, X.; Tian, X. B. *Inorg. Chem.* **2002**, *41*, 4560.
(19) Dellinger, T. M.; Braun, P. V. *Scr. Mater.* **2001**, *44*, 1893.
(20) Deng, H.; Wang, J.; Peng, Q.; Wang, X.; Li, Y. D. *Chem. Eur. J.* **2005**, *11*, 6519.
(21) Yang, P. D. *MRS Bull.* **2005**, *30*, 85.
(22) Lieber, C. M. *MRS Bull.* **2003**, *28*, 486.
(23) Pan, Z. W.; Dai, Z. R.; Wang, Z. L. *Science* **2001**, *291*, 1947.

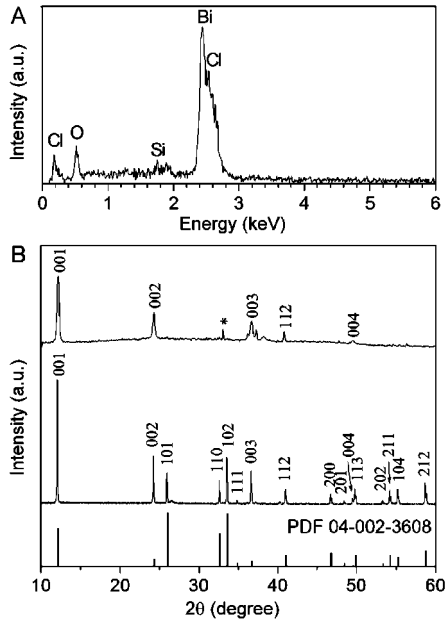

Figure 3. Chemical composition and crystal structure analyses of BiOCl nanostructures: (A) an EDS spectrum of the nanobelt film grown on a Si substrate. (B) XRD patterns of nanobelts (top) and platelets (middle) on the Si substrate with the reference diffractogram (bottom).

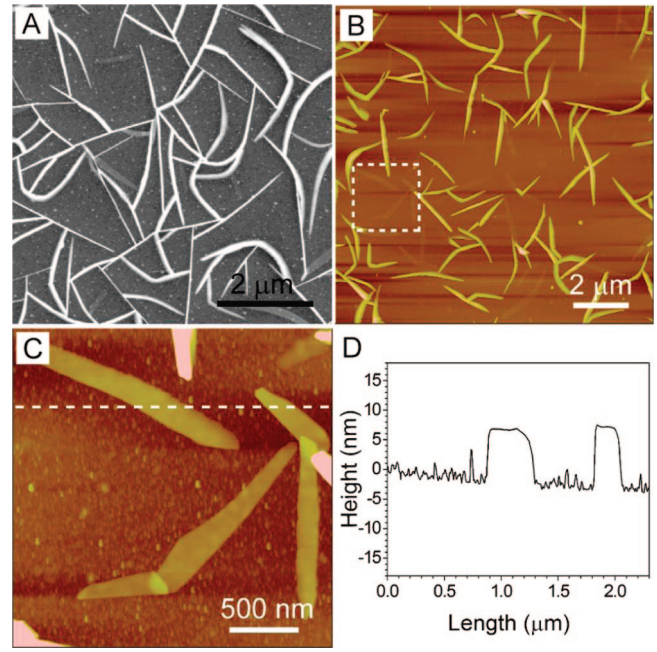

Figure 4. Thickness measurements of BiOCl nanobelts: (A) A representative SEM image of low density nanobelts grown on a bare Si ⟨100⟩ substrate. (B−D) AFM observations of the nanobelts.

temperature zones ranging from 250 to 150 °C in the tube furnace. The vapor source is the powder mixture of $AuCl_3$ and Bi placed at the temperature zone of 250 °C. The substrates are natively oxidized Si ⟨001⟩ substrate coated with Bi−Au catalyst film (20 nm Bi; 5 nm Au). Figure 2A show a large-area SEM image of a film of BiOCl nanostructures grown on the substrate placed at the hot temperature zone (∼250 °C). According to high-magnification SEM images (Figure 2B, inset, and Figure S1 in the Supporting Information), the film is made up of high-density NBs with thicknesses of 5−30 nm, widths of 100−200 nm, and lengths up to 1−2 μm.

At a lower temperature zone (∼200 °C), the shape of the BiOCl NBs evolves into two-dimensional (2D) flakes (Figure 2C). The flakes can further assemble into a roselike nanoflower in which each petal is a short flake grain as shown in Figure 2D. The diameter of the whole nanoflower is around 1−2 μm. At the cold zone of the tube furnace (∼150 °C), the vapor was quickly deposited as a densely packed film, which covered the whole substrate even on the quartz tube wall (Figure 2E). High-magnification SEM images reveal that the film consists of platelets. The platelet thickness ranges from 300 to 500 nm and widths extend up to several micrometers (Figure 2F and inset), which are much larger than those of the NBs grown at the hot zone. The platelets have straight edges with sharp corners, suggesting that they may terminate by faceted crystallographic planes.

(2) Chemical Composition and Crystal Structure. EDS was used to identify the composition of nanostructures. As shown in Figure 3A, EDS analysis confirms that the as-grown NBs consisted of Bi, O, and Cl. The Si peak comes from the Si substrate. Due to partial peak overlap for Cl and Bi, quantitative analysis of chemical composition could not be determined directly.

The crystal structure of the nanostructures was determined from the powder X-ray diffraction (XRD). As shown in Figure 3B, all the diffraction peaks in the XRD pattern of the platelet film sample can be indexed as a tetragonal structure of pure BiOCl (space group *P4/nmm*, No. 129, $a = 3.8830$ Å and $c = 7.3470$ Å, $Z = 2$; JCPDS 04-002-3608). In the XRD pattern of the NB film sample, most peaks can be assigned to the tetragonal structure of BiOCl. The additional peak at 33° marked by a star symbol comes from the ⟨200⟩ planes of Si substrate since the BiOCl NB film is thin and X-rays can penetrate into the Si substrate. In contrast to that of the bulk BiOCl (JCPDS 04-002-3608), the four peaks of the NBs (001), (002), (003), and (004) at 2θ of 12.04, 24.21, 36.65, and 49.60 have extraordinarily high intensity, which suggests that BiOCl nanostructures have an anisotropic shape. The XRD pattern of BiOCl nanoflowers sample can also be indexed as a tetragonal structure of pure BiOCl (Figure S2 in the Supporting Information).

(3) Thickness of Nanobelts. AFM observation can provide accurate height information on the BiOCl nanostructures. The samples for AFM observation are specially prepared by growing low density BiOCl NBs on a bare Si ⟨100⟩ substrate surface without Bi−Au catalyst film. A representative SEM image shows NBs with a length of 1−3 μm and width of 100−300 nm (Figure 4A). The NBs tend to interconnect forming a network on the substrate surface. A typical tapping-mode AFM topographic image of the same sample (Figure 4B) shows that networks of NBs randomly grew on the substrate surface with various orientations while individual NBs tended to lie on the substrate, consistent with SEM observations. A high-resolution AFM image shows some NBs lie flat on the substrate surface (Figure 3C). The section profile reveals the thickness is around 8.6 nm, corresponding to ∼11 layers of [Cl−Bi−O−Bi−Cl] sheets

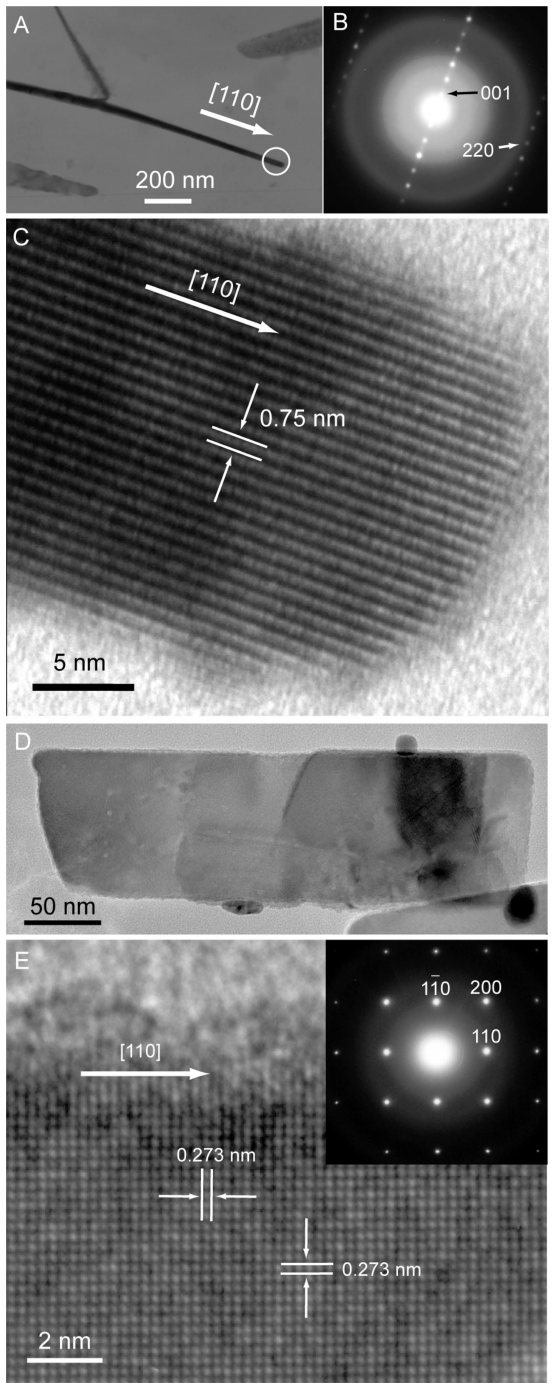

Figure 5. (A) Low-magnification TEM image of BiOCl nanobelts. (B, C) SAED pattern and HRTEM image of the end of the same nanobelts shown in (A) taken along the nanobelt plane. (D, E) TEM images and SAED pattern of the nanobelt taken along the [001] zone axis.

(Figure 3D). Extensive section analysis indicates the thickness of as-grown NBs ranges from 7 to 25 nm.

(4) Transmission Electron Microscopy (TEM). The microstructure of the BiOCl NB was further investigated with TEM. BiOCl NBs samples for TEM observations are directly grown on a 100 nm thick Si_3N_4 membrane TEM grid by using $AuCl_3$/Bi as vapor source under similar growth conditions as for AFM analysis. Figure 5A presents a bright-field TEM image of a NB with a branched NB, forming a Y-junction. The corresponding selected area electron diffraction (SAED) pattern of the main NB shows a regular spot pattern, confirming the single-crystalline nature of the NB with a [110] growth direction (Figure 5B). A high-resolution TEM (HRTEM) image (Figure 5C) of the same NB exhibits good crystalline and clear lattice fringes. The lattice spacing of the planes parallel to the growth direction is ~0.75 nm, as marked in the image, agreeing well with the spacing of the (001) planes of BiOCl. The results confirm that BiOCl NBs consists of sheets stacked together along the *c*-axis, as shown in Figure 1. The thickness of the NB is ~21 nm, corresponding to 28 layers of sheets. In contrast to Y-junction NBs, a single NB tends to lie down with the *c*-axis parallel to the electron beam when it was grown or transferred onto the TEM substrates, as shown in Figure 5D. The HRTEM image (Figure 5E) shows that it is single-crystalline, and the spacing of the lattice planes parallel or perpendicular to the NB long axis is the 0.273 nm, consistent with the spacing of (110) planes of the BiOCl. The growth direction of the NB is the [110] direction, confirmed by the corresponding SAED pattern (Figure 5E inset). Our extensive TEM observations reveal the growth direction of the NBs is along the [110] without exception, which is different from the growth direction of nanostructures prepared by solution phase synthesis.[20]

(5) Growth Mechanism. BiOCl NBs, nanoflowers, and platelets have been successfully grown via vapor transport reactions. We observed the morphological and structural evolution of the reaction products at different growth temperatures. In order to understand the growth mechanism behind the formation of these nanostructures, we investigated the effect of the evaporation source and catalyst.

The BiOCl bulk compound is known to form by heating $BiCl_3$ in air or by hydrolysis of $BiCl_3$.[24,25] In addition to the $AuCl_3$/Bi source used in our chemical vapor deposition (CVD) approach, $BiCl_3$ powder can also function as a cost-efficient source for the high-yield growth of BiOCl nanostructures. $BiCl_3$ powder is very hygroscopic and easily hydrolyzable in water.[24] The surface of the $BiCl_3$ powder hydrolyzed with several drops of deionized water was loaded in the tube furnace for the growth of BiOCl nanostructures. Control experiments with anhydrous $BiCl_3$ in the dry tube furnace system did not yield any BiOCl nanostructures, indicating that the presence of trace water is critical for the growth of BiOCl nanostructures. As shown in Figure 6A, a representative SEM image shows a high density BiOCl nanoflake film grown on a Si substrate initially coated with a Bi/Au film (20 nm Bi, 5 nm Au) in the ~220 °C zone. From the zoom-in image of the BiOCl film (Figure 6B), the flakes intersect and aggregate together to form a complex network-like structure. The size of the flakes is about several micrometers across and several tens of nanometers in thickness. EDX analysis and powder XRD pattern confirm the composition and tetragonal phase of pure BiOCl (Figures S3 and S4 in the Supporting Information).

BiOCl nanostructures were synthesized by using either a $AuCl_3$/Bi or $BiCl_3$ source. The $AuCl_3$ source begins to decompose to AuCl and Cl_2 at around 160 °C or in light

(24) Patel, A. R.; Shivakumar, G. K.; Rao, K. V. *Thin Solid Films* **1977**, *41*, L11.
(25) Silvestri, V. J.; Sedgwick, T. O.; Landermann, J. B. *J. Cryst. Growth* **1973**, *20*, 165.

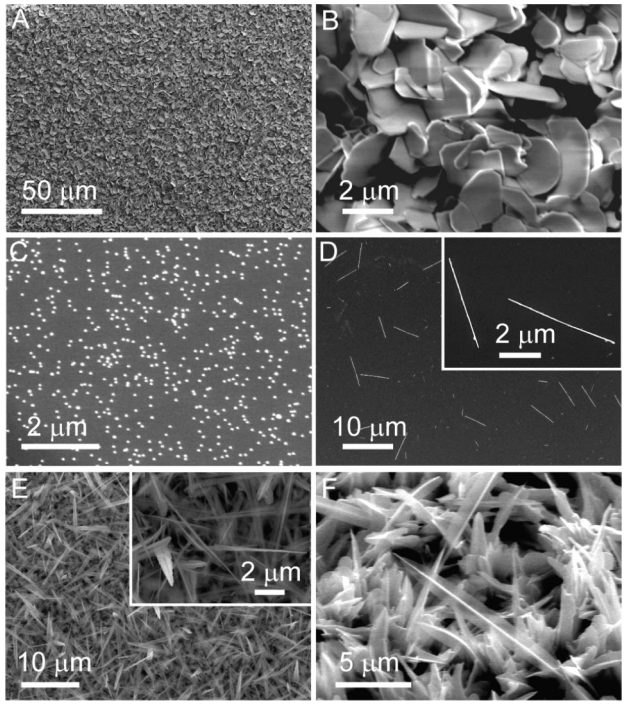

Figure 6. SEM images of BiOCl nanostructures growth by using $BiCl_3$ source: (A, B) SEM images of high density of BiOCl nanoflakes film grown on a Si substrate first coated with Bi/Au film; (C) growth results using Si substrate coated with Au nanoparticles; (D) BiOCl nanowires grown on a bare Si substrate using additional Bi powder in the $BiCl_3$ source. (E, F) Top-view and side-view of free-standing BiOCl nanobelts grown on a glass slide substrate previously coated by 5 nm Bi and 5 nm Au films, respectively.

according to the following reaction: $AuCl_3 \rightarrow AuCl + Cl_2$. At 250 °C, the Cl_2 vapor reacts with Bi quickly and makes $BiCl_3$ (melting point: 234 °C, bp ~430).[26] The $BiCl_3$ is vaporized at 250 °C and carried by inert gas downstream where it is hydrolyzed to BiOCl following the reaction with trace H_2O gases according to the reaction $BiCl_3 + H_2O \rightarrow BiOCl + 2HCl$. The trace H_2O may come from the vapor source because both $AuCl_3$ and $BiCl_3$ are very hygroscopic before loading into the system. The formation mechanism of the NB and flake shape is attributed to the anisotropic bonding of the BiOCl layered structure. In BiOCl, the [110] direction is the fastest growth direction and the [001] is the slowest due to the weak *c*-axis bonding. Indeed, one-dimensional (1D) NB and 2D flake structures have been observed in hydrothermal methods.[17,20]

We believe the growth of 1D BiOCl NBs in our CVD approach is based on a vapor−liquid−solid (VLS) mechanism. The VLS mechanism has been used extensively for the growth of 1D IV, II−VI, III−V, and III−VI semiconductor nanostructures, in which metal droplets catalytically enhance the growth of 1D nanostructures.[21,22,27,28] As already mentioned above, using the Si substrates coated with Bi/Au film, high-yield BiOCl nanostructures were successfully synthesized. Si substrates coated with Sn/Au film (20 nm Sn, 5 nm Au) were also found to product BiOCl nanostructures with high deposition density (data not shown). We believe that the low-melting-point metal, such as Bi and Sn, plays important role in the growth of 1D nanostructures of BiOCl. A bare Si substrate or Si substrate coated with Au nanoparticles (20 nm in diameter) did not yield any BiOCl nanostructures under otherwise identical conditions (Figure 6C and Figures S5 and S6 in the Supporting Information). In contrast, BiOCl nanowires were produced on the bare Si substrate once additional Bi powder was placed in the $BiCl_3$ source (Figure 6D). These results indicate that the presence of Bi is critical for the growth of BiOCl nanostructures based on the VLS mechanism.

An important feature in VLS growth is the appearance of metal catalyst particles at the tips of NWs. However, the majority of the BiOCl NBs usually show a tapered shape at the tip (Figure 5C) without the presence of metal catalyst. We think that the absence of catalyst nanoparticles on most NBs after synthesis might be due to the shrinkage and disappearance of Bi catalysts through evaporation because Bi has a high vapor pressure. Another possible mechanism is the consumption of Bi through a chemical reaction with Cl_2 or trace O_2 because Bi metal is used as both a source and a catalyst for BiOCl growth. A similar process has been recently reported that used Bi as the catalyst and source for the growth of Bi_2O_3 nanostructures.[29] A self-catalyzed VLS mechanism was proposed to be responsible for nucleation and a vapor−solid (VS) process for the 1D nanostructure growth.[29,30]

We investigated the mechanism behind the formation of NB aggregates and nanoflowers. The liquid alloy cluster or defects have previously been suggested as an "active site" for preferential adsorption of reactant from the vapor phase and as the nucleation site for crystallization. The existing Bi vapor from the evaporation of Bi powder source in the subsequent growth process continuously condenses to small liquid droplets onto the preformed NBs and serves as active sites to nucleate and grow new branches.

Au−Bi film on the Si substrate can form liquid alloy droplets at 250 °C according to the Au−Bi phase diagram (eutectic temperature: 241.1 °C).[31] Each eutectic alloy droplet directs the growth of an individual NB. High density liquid alloy droplets on the substrate may be responsible for free-standing and densely packed NB arrays.

Single-crystalline BiOCl platelets have been successfully grown from the BiOCl vapor at the source temperature of 720 °C and the deposition temperature of 600 °C via a physical vapor deposition (PVD) process.[32] Compared with the PVD method, however, our CVD synthesis requires relatively low temperatures (≤250 °C) to carry out the VLS or VS transformations associated with catalytic growth. The low-temperature growth offers a mild way of producing BiOCl nanostructures on many types of substrates, including

(26) Skinner, H. A.; Sutton, L. E. *Trans. Faraday Soc.* **1940**, *36*, 681.
(27) Peng, H. L.; Meister, S.; Chan, C. K.; Zhang, X. F.; Cui, Y. *Nano Lett.* **2007**, *7*, 199.
(28) Peng, H. L.; Schoen, D. T.; Meister, S.; Zhang, X. F.; Cui, Y. *J. Am. Chem. Soc.* **2007**, *129*, 34.
(29) Qiu, Y. F.; Liu, D. F.; Yang, J. H.; Yang, S. H. *Adv. Mater.* **2006**, *18*, 2604.
(30) Kar, S.; Pal, B. N.; Chaudhuri, S.; Chakravorty, D. *J. Phys. Chem. B* **2006**, *110*, 4605.
(31) Okamoto, H.; Massalski, T. B. *Au-Bi (Gold-Bismuth), Binary Alloy Phase Diagrams*, II ed.; 1990; Vol. 1, ASM International: Materials Park, OH, p 343.
(32) Ganesha, R.; Arivuoli, D.; Ramasamy, P. *J. Cryst. Growth* **1993**, *128*, 1081.

glass slides. Figure 6E exhibits the high density leaflike BiOCl NBs grown on a glass slide substrate previously coated by 5 nm Bi and 5 nm Au films. The lengths of the leaflike NBs are mainly several micrometers. The side-view SEM image (Figure 6F) shows most of the NBs are free-standing.

Conclusion

In conclusion, a facile vapor-phase synthesis route was developed for the direct growth of high quality BiOCl nanostructure films on various substrates by thermal evaporation of a $AuCl_3$/Bi mixture or $BiCl_3$ at low-temperature (250 °C). BiOCl nanostructures could be directly grown on various substrates as a densely packed array. BiOCl nanostructures exhibit a variety of morphologies including nanowires, nanobelts, nanoflowers, nanoflakes, and platelets. We achieved control of these morphologies by choosing the deposition temperature, evaporation source, and catalysts.

Acknowledgment. We acknowledge support from U.S. DOE under the Award Number DE-FG36-08GO18005. Y.C. acknowledges the Stanford Global Climate Energy Project. C.K.C. acknowledges support from a NSF Graduate Fellowship and Stanford Graduate Fellowship.

Supporting Information Available: SEM images, TEM image, EDS spectrum, and XRD patterns (PDF). This material is available free of charge via the Internet at http://pubs.acs.org.

CM802041G